

UCR: An Unclonable Environmentally Sensitive Chipless RFID Tag For Protecting Supply Chain

KUN YANG, ULBERT BOTERO, HAOTING SHEN, DAMON L. WOODARD, DOMENIC FORTE, and MARK M. TEHRANIPOOR, University of Florida

Chipless Radio Frequency Identification (RFID) tags that do not include an integrated circuit (IC) in the transponder are more appropriate for supply-chain management of low-cost commodities and have been gaining extensive attention due to their relatively lower price. However, existing chipless RFID tags consume considerable tag area and manufacturing time/cost because of complex fabrication process (e.g., requiring removing or shorting some resonators on the tag substrate to encode data). Worse still, their identifiers (IDs) are deterministic, clonable, and small in terms of bitwidth. To address these shortcomings and help preserve the cold chain for commodities (e.g., vaccines, pharmaceuticals, etc.) sensitive to temperature, we develop a novel unclonable environmentally sensitive chipless RFID (UCR) tag that intrinsically generates a unique ID from both manufacturing variations and ambient temperature variation. A UCR tag consists of two parts: (i) a certain number of concentric ring slot resonators integrated on a certain laminate (e.g., TACONIC TLX-0), whose resonance frequencies rely on geometric parameters of slot resonators and dielectric constant of substrate material that are sensitive to manufacturing variations, and (ii) a stand-alone circular ring slot resonator integrated on a particular substrate (e.g., grease) that will be melted at a high temperature, whose resonance frequency relies on geometric parameters of slot resonator, dielectric constant of substrate material, and ambient temperature. UCR tags have the capability to track commodities and their temperatures in the supply chain. The area of UCR tag is comparable to regular quick response (QR) code. Experimental results based on UCR tag prototypes have verified their uniqueness and reliability.

CCS Concepts: • **Security and privacy** → **Hardware security implementation**;

Additional Key Words and Phrases: Chipless RFID tag, cold chain, irreversible temperature tracking, uniqueness, unclonability

ACM Reference format:

Kun Yang, Ulbert Botero, Haoting Shen, Damon L. Woodard, Domenic Forte, and Mark M. Tehranipoor. 2018. UCR: An Unclonable Environmentally Sensitive Chipless RFID Tag For Protecting Supply Chain. *ACM Trans. Des. Autom. Electron. Syst.* 23, 6, Article 74 (November 2018), 24 pages.

<https://doi.org/10.1145/3264658>

An earlier version of this article was published in *Proceedings of the 2016 IEEE International Symposium on Hardware Oriented Security and Trust (HOST'16)* [34].

Authors' addresses: K. Yang, U. Botero, H. Shen, D. L. Woodard, D. Forte, and M. M. Tehranipoor, Florida Institute for Cybersecurity Research, University of Florida, 601 Gale Lernerand Dr., P.O. Box 116550, Gainesville, FL 32611; emails: {k.yang, jbot2016, htshen, dwoodard, dforte, tehranipoor}@ufl.edu.

Permission to make digital or hard copies of all or part of this work for personal or classroom use is granted without fee provided that copies are not made or distributed for profit or commercial advantage and that copies bear this notice and the full citation on the first page. Copyrights for components of this work owned by others than ACM must be honored. Abstracting with credit is permitted. To copy otherwise, or republish, to post on servers or to redistribute to lists, requires prior specific permission and/or a fee. Request permissions from permissions@acm.org.

© 2018 Association for Computing Machinery.

1084-4309/2018/11-ART74 \$15.00

<https://doi.org/10.1145/3264658>

1 INTRODUCTION

Today's supply chain is remarkably complex, diverse, and extensive. While globalization has optimized resource allocation and reduced manufacturing cost, it also exposes the supply chain to more risks such as theft, counterfeiting, mishandling, improper storage, and so on. Not only do these risks compromise the profits and reputations of manufacturers, distributors, and retailers, but they also pose a threat to human health and asset safety. In 2014, there were more than 23,000 seizures of counterfeit and pirated goods worth an estimated value of \$1.2 billion at America's ports of entry, according to U.S. Customs and Border Protection (CBP) and U.S. Immigration and Customs Enforcement's Homeland Security Investigations (HSI) [6]. In 2015, the FreightWatch International Supply Chain Intelligence Center (FWI SCIC) recorded a total of 754 cargo thefts in the United States with an average loss of \$184,101 per incident [5]. In March 2016, a hospital pharmacist and her daughter in eastern Shandong province of China were found to have sold 2 million doses of improperly stored vaccines with an estimated value of \$88 million [23, 24]. The vaccines in question had been stored at room temperature, instead of being kept refrigerated as required, which could have compromised their effectiveness [23, 24].

Track-and-trace measures lay the foundation for an improved supply chain by enabling supply-chain owners and/or participants to systematically detect and control counterfeiting, theft, mishandling, improper storage, and so on, but existing techniques are quite costly, inconvenient, unreliable, or insecure. Barcodes [32] have traditionally been employed to track and trace commodities in the supply chain. QR codes [11] with greater storage capacity have also been put into use more recently. Encryption can prevent unauthorized information access to QR codes [4]. However, both barcodes and QR codes are vulnerable to cloning attack because of visibility and controllability of pixel information (even though the adversary cannot retrieve the specific content from an encrypted QR code). Other disadvantages (e.g., requirement of individual scanning, direct line-of-sight, and close proximity to scanner, etc.) also badly impact their overall utility.

Radio Frequency Identification (RFID) is widely believed to be a promising substitute of barcodes/QR codes. Wal-Mart and the United States Department of Defense have published requirements that their vendors should attach RFID tags to all shipments to enhance supply-chain management [30]. Compared with traditional optical labels, an RFID-based track-and-trace system has many engaging features—enables batch scanning, does not require direct line-of-sight for access, and needs less human involvement to collect data—making automatic track and trace possible. A series of encryption algorithms (e.g., advanced encryption standard (AES), elliptic curve cryptography (ECC), etc.) have been proposed to enhance the security and privacy of RFID communication protocols [8, 14]. The authors in Reference [10] proposed to replace cryptography with ultra wideband (UWB) modulation in secure RFID. Silicon physical unclonable functions (PUFs) have also been proposed to be integrated in RFID ICs for anti-counterfeiting and security purposes [7, 15]. However, the relatively higher price of IC-based RFID tags makes them inappropriate for protecting the supply chain of low-cost commodities.

Recently, chipless RFID tags [19, 21, 22] without microchips have been gaining attention due to their relatively lower price, extremely low power requirement, and less sensitivity to temperature. Compared with IC-based RFID tags, chipless RFID tags have the following advantages: (i) the extremely low price (as low as 0.1 cents) makes them more appropriate to be used in the supply chain of low-cost commodities; (ii) elimination of tag memory shelters them from denial-of-service (DoS) attack carried out in the form of overwriting tag memory; and (iii) chipless RFID tags can be directly printed on the products or their packages with conductive 3D printing materials. Existing chipless RFID tags, however, require either removing or shorting some resonators (i.e., spirals or patch slots) on the tag substrate to represent data [19, 20]. When one resonator is removed or shorted, its corresponding resonance point will be either removed from the frequency response

spectrum or shifted outside of the frequency range of interest. One bit is encoded to “1” when the corresponding resonance point exists at a specific frequency, and “0” when the resonance point disappears or vice versa. Removing resonators will waste tag area. Shorting resonators ensures the same layout with all the resonators shorted can be used to produce different chipless RFID tags. When encoding data, the shorting can be removed using laser cutting or conventional etching techniques. Both removing and shorting procedures will increase the manufacturing time/cost. For the same designs, the IDs generated by current chipless RFID tags are deterministic and predictable. As a result, they are vulnerable to cloning attack. Other disadvantages such as small ID size (usually not exceeding 35 bits) and considerable tag area also impact their utility.

Some commodities (e.g., pharmaceuticals, food, beverages, etc.) have to be kept at an appropriate temperature during distribution; otherwise, their efficacy, quality, or flavor will be undermined. For example, vaccines have to be distributed in the cold chain (i.e., maintaining proper temperatures during storage and transportation) to preserve potency. However, there is no cost-effective solution for tracking the temperature of commodity items in the supply chain.

To mitigate the aforementioned limitations of existing solutions and establish reliable visibility into supply-chain status, we propose a novel unclonable, environmentally sensitive chipless RFID (UCR) tag. UCR tag in essence is a unique object [25] that, on measurement by an external apparatus, exhibits a small, fixed set of inimitable analog properties that are not the same as any other entity. We take advantage of the uncontrollable process variations during tag fabrication to generate a unique and unclonable ID that can be used for tracking and tracing commodities (e.g., food, beverages, pharmaceuticals, vaccines, newspapers, magazines, etc.) in the supply chain. We have also developed a cost-effective approach to track the temperatures of commodities in the supply chain. Other than improving supply-chain management, UCR tags can also be implanted into passports, driving licenses, and license plates to help verify the identities of citizens and vehicles. Furthermore, a UCR tag has the capability to broaden the scope of the Internet of Things (IoT) [18, 31, 33] by enabling many non-electronic products to be connected to the network. A UCR tag consists of two parts: (i) a certain number of concentric ring slot resonators integrated on a certain laminate (e.g., TACONIC TLX-0), whose resonance frequencies depend on geometric parameters of slot resonators and dielectric constant of substrate material that are sensitive to manufacturing variations, and (ii) a stand-alone circular ring slot resonator integrated on a particular substrate (e.g., grease) that will be melted at a high temperature, whose resonance frequency depends on geometric parameters of the slot resonator, the dielectric constant of the substrate material, and the ambient temperature. To the best of our knowledge, this is the first time that manufacturing variations have been exploited to generate the unique ID from a chipless RFID tag. The area of the UCR tag is comparable to regular QR code. Our main contributions are as follows:

- We theoretically derive the sensitivity of slot resonance frequency towards the variances of slot geometric parameters and substrate dielectric constant and take advantage of this sensitivity to develop a new type of unclonable chipless RFID tags that carry unique IDs.
- We develop a novel cost-effective approach for tracking the temperatures of commodities in the supply chain.
- We propose a novel and efficient look-up method that accelerates the authentication process of UCR tags.
- We fabricate UCR tag prototypes and evaluate their performance in the lab environment under several conditions. We also explore and compare a variety of supervised and unsupervised methods for identifying tags based on their UCR responses.

The remainder of this article is organized as follows: Section 2 introduces prior work concerning chipless RFID tags and temperature monitoring, Section 3 discusses the necessary preliminaries for

developing chipless RFID tags. Section 4 describes the proposed UCR tags in detail and how they can generate unique and unclonable IDs and track the temperature of commodities in the supply chain. Section 5 defines the adversarial model. In Section 6, we evaluate the performance of tags in the lab environment based on our fabricated UCR tag prototypes. We also analyze the resilience of UCR system to the potential attacks in this section. Finally, we give concluding remarks and point out future research directions in Section 7.

2 RELATED WORK

Two areas of prior work have particular relevance to UCR: chipless RFID tags and temperature monitoring.

Chipless RFID Tags: Chipless RFID tags can be divided into three classes: (i) time-domain reflectometry- (TDR) based chipless tags [12]; (ii) spectral signature-based chipless tags [19, 20]; and (iii) amplitude/phase backscatter modulation-based chipless tags [21]. Because of page limit, we review only closely related spectral signature-based chipless tags.

The authors of References [19, 20] developed a fully passive printable chipless RFID tag by placing multiple spiral resonators close to the IC that connects two cross-polarized UWB monopole antennas (one transmitter and one receiver). Spiral resonators with different dimensions will exhibit different resonance frequencies. Data encoding is implemented by either removing the spiral or shorting its turns. Three-dimensional (3D) printing techniques will preserve the layout with all of the spirals shorted and when encoding data the shorting can be removed using laser cutting or conventional etching techniques. The bit width of chipless RFID implemented in this approach will be equal the number of spiral resonators. Correspondingly, the tag area will be proportional to the bit width of chipless RFID, which is undesirable.

Closest to our work is the slot-loaded dual-polarized chipless RFID tag proposed in Reference [16], where four rectangular metallic patches loaded with multiple slot resonators are used to construct the tag. The logic state of a bit is changed simply by shorting the slot at the corner point, which will shift the resonance frequency of the slot resonator out of the frequency band of interest. To reduce the mutual coupling between the slots, slots with the same polarization for adjacent frequencies are placed alternatively into two patches. To double the number of bits within the same frequency bandwidth, two similar sets are placed in horizontal and vertical polarizations. Since multiple slots can be placed into the same patch, the tag area is observably smaller than the above-mentioned spiral resonator-based tag. One drawback of this technique is that the cross-polarized response will be too small to recognize if the tag is rotated by an angle larger than a certain limit.

Removing or shorting the resonator (i.e., spiral or patch slot) is necessary for both techniques to alter the logic state of the corresponding bit. The manufacturing cost will be unacceptable if different layouts with different resonator shorting states are employed to fabricate the tags. Although the layout can be preserved with all the resonators shorted and when encoding data the shorting can be removed using laser cutting or etching techniques, the manufacturing time will be significantly increased. For a design with specific parameters, the IDs generated in both ways are deterministic and predictable, making these chipless RFID tags vulnerable to cloning attack.

Temperature Monitoring: The authors of Reference [9] developed a passive wireless temperature sensor based on a time-coded UWB chipless RFID tag. It consists of an UWB antenna connected to a delay line that is loaded with a resistive temperature sensor. The sensor modulates the amplitude of the backscattered signal as a function of the temperature. The authors of Reference [3] implemented a chipless RFID temperature sensor by replacing regular substrate material of spiral resonator with Stanyl polyamide that has a linear variation of dielectric constant with temperature. The authors of Reference [29] proposed another chipless RFID tag with

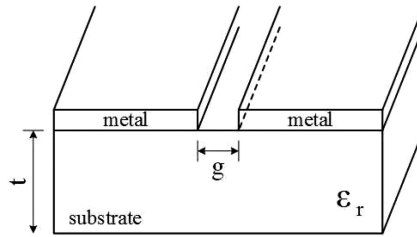


Fig. 1. Cross-section view of slot-line resonator.

temperature-sensing capability. To make a resonator sensitive to the temperature, a material based on silicon nanowire is deposited on the tag surface. When the temperature alters the conductivity of the material is changed so that the field lines are rearranged and a small frequency shift can be observed. However, all the above-mentioned temperature-sensing mechanisms cannot simply be adapted to track the temperatures of commodities in the supply chain due to the lack of memory. Their shifts of resonance frequencies caused by temperature variances are reversible. When the temperature returns to its normal level, the resonance frequency will restore as well.

To mitigate the shortcomings of previous work, we develop a new unclonable environmentally sensitive chipless RFID (UCR) tag that intrinsically generates a unique ID from both manufacturing variations and ambient temperature variation. An extreme temperature change will cause the latter to permanently change its response.

3 PRELIMINARIES

The preliminaries (i.e., notch frequency sensitivity of slot resonator as shown in Figure 1 towards slot geometric parameters and substrate dielectric constant, and slot shape selection) for developing chipless RFID tags have been thoroughly discussed in an earlier version of this article [34]. The analyses presented in Reference [34] can be summarized as follows:

- As shown in Figure 2, notch frequency is sensitive to the variances of slot geometric parameters and substrate dielectric constant. All three notch frequency sensitivities (i.e., $\frac{\partial f_s}{\partial g}$, $\frac{\partial f_s}{\partial t}$, and $\frac{\partial f_s}{\partial \epsilon_r}$, where f_s , g , t , and ϵ_r , respectively, refer to the notch frequency of slot-line resonator, air gap, substrate thickness, and dielectric constant of substrate material) appear linear to the variance of notch frequency in the frequency range of UWB (i.e., from 3.1 to 10.6 GHz). Compared with substrate thickness and patch thickness, notch frequency is more sensitive to the variances of air gap and substrate dielectric constant. High-frequency resonance points are more sensitive to the variances of slot parameters than low-frequency resonance points. Air gap has little impact on the sensitivity of notch frequency to the variance of substrate thickness. The curves of $\frac{\partial f_s}{\partial t}$ with the same substrate thickness and dielectric constant of substrate material but different air gaps are overlapping with each other.
- Circular ring shaped slot resonators are the most appropriate candidates for composing our proposed UCR tag due to the following three reasons:
 - Circular ring shaped slot resonator does not require the incident plane wave to be in perfect alignment with the tag.
 - The fabrication accuracy of circular ring shaped slot's geometric parameters is more difficult to manipulate than slots of other shapes, which is conducive to generating larger variations during manufacturing. This will result in larger variations in the signatures of chipless RFID tags, making them more suitable as unique identifiers.

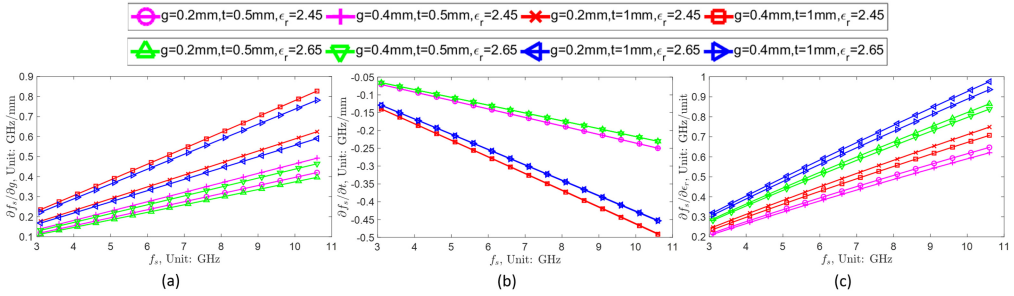


Fig. 2. Sensitivity of notch frequency to slot parameters at different frequencies: (a) sensitivity to air gap ($\frac{\partial f_s}{\partial g}$), (b) sensitivity to substrate thickness ($\frac{\partial f_s}{\partial t}$), and (c) sensitivity to dielectric constant ($\frac{\partial f_s}{\partial \epsilon_r}$).

—The same number of concentric ring slot resonators occupy less tag area than other slot resonator geometries such as split square shaped slot resonator. In other words, for the given tag area, more concentric ring slot resonators can be integrated on the tag substrate, which is conducive to increasing the uniqueness of tag identifier. If the tag consists of N slot resonators, then the tag identifier will be composed of N analog values (i.e., N fundamental resonance points in the frequency response spectrum). If each analog value is converted to M digital bits, then there will be altogether 2^{NM} possible combinations.

4 UCR SYSTEM

The proposed UCR system is presented in this section. We first describe the architecture and working principle of UCR system and then introduce a novel and efficient look-up method that could be used at the authentication phase to quickly determine whether the tag under authentication (TUA) belongs to the database. Last, we discuss the potential application scenario.

4.1 Architecture and Working Principle

Figure 3 illustrates the architecture of UCR system. A UCR tag consists of two parts: (i) a certain number of concentric ring slot resonators integrated on a certain substrate (e.g., TACONIC TLX-0), whose resonance frequencies depend on slot geometric parameters and substrate dielectric constant that are sensitive to manufacturing variations, and (ii) a stand-alone circular ring slot resonator integrated on a particular substrate (e.g., grease) that will be melted at a high temperature, whose resonance frequency depends on slot geometric parameters, substrate dielectric constant, and ambient temperature. UCR part I is in charge of generating a unique, unclonable identifier for tracking and tracing commodities in the supply chain. UCR part II is in charge of tracking the temperatures of commodities in the supply chain.

4.1.1 UCR Part I (Unique Identifier). Figure 4 shows the first part of UCR tag that consists of a certain number of concentric ring slot resonators integrated on a certain laminate (e.g., TACONIC TLX-0). When we stimulate the UCR tag with an UWB plane wave, as illustrated in Figure 3(a), the number of fundamental resonance points in the frequency response spectrum will correspond to the number of slot resonators. A typical UWB RFID reader or a smart phone that integrates necessary hardware (i.e., antenna, analog front-end, analog-to-digital converter, etc.) will be responsible for providing the UWB plane wave and capturing the frequency response spectrum. These resonance points are independent of each other. Because of process variations during tag fabrication, the slot parameters (i.e., trace width, air gap, substrate thickness, and substrate material dielectric constant) of each resonator will shift away from their design values.

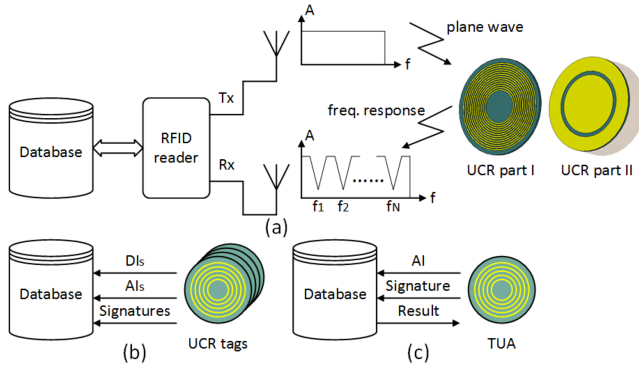


Fig. 3. UCR system: (a) working principle, (b) enrollment, and (c) authentication.

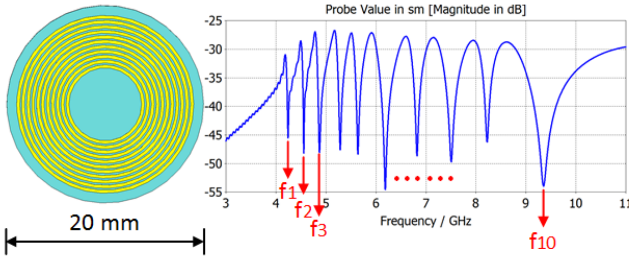


Fig. 4. UCR part I (unique identifier).

Table 1. PCB Manufacturing Tolerances

PCB Manufacturer	Trace Width/Air Gap Tolerance	PCB Thickness Tolerance
Advanced Circuits	max($\pm 20\%$, $\pm 0.002''$)	max($\pm 10\%$, $\pm 0.005''$)
Sunstone	$\pm 20\%$	$\pm 10\%$
Sierra Circuits	$\pm 0.001''$	$\pm 10\%$
Precision PCBs	$\pm 20\%$	$\pm 0.005''$
RUSH PCB	$\pm 0.005''$	$\pm 10\%$

Table 1 illustrates the manufacturing tolerances of five major printed circuit board (PCB) manufacturers in the United States. For the trace width and air gap, the maximum deviation between design value and measured value can be as large as 20%. PCB thickness will typically have a tolerance of 10%. Table 2 shows the dielectric constant (ϵ_r) tolerances of six typical high-frequency laminates. The dielectric constant tolerances can range from 1.33% to 3.49%. According to the analysis in Section 3 (see Figure 2), the resonance frequency of each slot resonator will shift away from its design value due to the variances of slot parameters and substrate dielectric constant. Because of the randomness of process variation, the frequency signature of each UCR tag will be unique and different from each other. The vector (f_1, f_2, \dots, f_N) will be used as the identifier of each tag, where f_i represents the resonance frequency of the i_{th} slot resonator. The proposed UCR tag is unclonable, since the adversaries cannot easily model the uncontrollable process variations during tag fabrication. For a UCR tag with 10 slot resonators, its diameter could be as short as 20 mm, which is comparable to the dimension of QR code.

Table 2. PCB Laminate ϵ_r Tolerances

Supplier	Laminate	ϵ_r	ϵ_r Tolerance
TACONIC	RF-30	3.00	± 0.10
TACONIC	TRF-43	4.30	± 0.15
TACONIC	TLX-0	2.45	± 0.04
ROGERS	RO3003	3.00	± 0.04
ROGERS	RO4350B	3.48	± 0.05
ROGERS	RT/Duroid 6006	6.15	± 0.15

Because of noise interference and angle variation of incident plane wave, the signatures captured from the same tag may be slightly different for different measurements. Euclidean distance between two vectors $\vec{v}_i^j = (f_1^j, f_2^j, \dots, f_N^j)$ and $\vec{v}_i^k = (f_1^k, f_2^k, \dots, f_N^k)$ will be used to determine whether these two vectors belong to the same tag, where \vec{v}_i^j and \vec{v}_i^k indicate the signatures of the i_{th} tag measured at times j and k . The Euclidean distance (ED) between \vec{v}_i^j and \vec{v}_i^k can be calculated as follows:

$$ED_i^{j,k} = |\vec{v}_i^j - \vec{v}_i^k| = \sqrt{\sum_{r=1}^N (f_r^j - f_r^k)^2}. \quad (1)$$

Two signatures are determined to belong to the same tag if their Euclidean distance is not larger than the maximum intra-tag Euclidean distance obtained at the enrollment phase.

Euclidean distance-based tag recognition, which requires only a small amount of computation, is straightforward and time efficient. However, the intrinsic disadvantage of this tag recognition method is that it does not fully exploit the tag frequency spectrum information. The tag recognition accuracy can be remarkably improved if the vast majority of tag frequency spectrum information is exploited. Supervised machine learning provides a method of guiding the UCR system to correctly learn and classify the features that differentiate the tags from one another. Since supervised machine learning takes advantage of the vast majority of tag frequency spectrum information rather than only rely on resonance points, the recognition accuracy could be increased. One popular supervised learning technique is the linear discriminant analysis (LDA) [17] classifier. By maximizing the variance between different tag measurements and minimizing the variance within the same tag measurements, the classifier is able to distinguish between different tags by focusing on the most discriminant features, a la principal component analysis (PCA) [27]. Furthermore, the classification algorithm also serves as a method of dimensionality reduction. The computation of the transformation matrix for LDA is reliant on being able to compute the inverse within tag scatter matrix, which means the matrix must be non-singular. However, in practice the opposite is often the case with high-dimensional data where the size of the dataset is smaller than its dimensionality. This is the case for our experiments in Section 6 but may not be so in practical application where a database could contain as many as millions of tags. For this reason, PCA is still necessary for not only dimensionality reduction but also to ensure the resultant matrices after projection are non-singular. Applying PCA prior to computing LDA is a good practice regardless of the size of the dataset, since it helps with avoiding overfitting. Therefore, the procedure for implementing a supervised machine-learning-based tag authentication system is as follows:

Step 1: Compute the principal components of the tag dataset to be enrolled.

Step 2: Project the tag spectra into reduced dimensional space using computed principal components. This also ensures non-singular matrices for subsequent LDA computation.

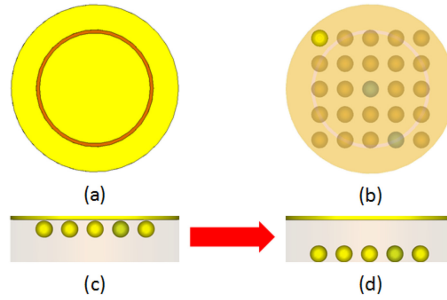


Fig. 5. UCR part II (temperature tracker): (a) top view, (b) top perspective view, (c) side view before grease is melted, and (d) side view after grease is melted.

Step 3: Apply LDA to projected data to compute transformation matrix that can be used for LDA projection and classification.

Step 4: Apply LDA transformation matrix to PCA projected tag spectra and enroll resultant LDA projected tag signatures into database.

Step 5: Use principal components from **Step 1** to project the spectrum of tag under authentication (TUA) to reduced dimensional space. Then apply LDA transformation matrix computed in **Step 3** to PCA projected TUA spectrum. If in the projected space TUA has the minimum distance with an enrolled tag compared with all the remaining tag entries, and that distance is smaller than a threshold d_{th} computed from the equal error rate (EER) of the enrolled tag database, then we determine that TUA matches with this tag entry; otherwise, we determine that TUA does not belong to the database.

However, a potential drawback of this approach is that the computational complexity increases as the size of enrollment increases. For every new enrollment, PCA and LDA would need to be reapplied. For PCA the principal components that capture the most variance at a reduced dimensionality would need to be recalculated. For LDA the projections that maximize the variance between PCA projected different tag measurements and minimize the variance within PCA projected same tag measurements would need to be recalculated. This would be inconvenient and computationally intensive for large datasets.

By supplanting the supervised learning methodology with an unsupervised approach, there would be a tradeoff in a decrease in accuracy for increased computational savings and ease in new tag enrollments. The unsupervised approach would be to simply find a set of features that distinguish tags from one another, such as their resonance points, and merely perform distance calculations or compute the similarity between feature vectors. The procedure for implementing an unsupervised machine-learning-based tag authentication system is as follows:

Step 1: During the *enrollment phase*, extract feature vectors (e.g., the set of resonance points) from all UCR tags and store them in the database.

Step 2: During the *authentication phase*, extract feature vector from TUA.

Step 3: Look up tag entry that has the minimum distance or maximum similarity with TUA in the database. If the minimum distance is smaller than a threshold d_{th} computed from the EER of the enrolled tag database, then we determine that TUA matches with this tag entry; otherwise, we determine that TUA does not belong to the database.

4.1.2 UCR Part II (Temperature Tracker). As shown in Figure 5, the second part of the UCR tag is a stand-alone circular ring slot resonator integrated on a particular substrate (e.g., grease) that will be melted at a high temperature. The resonance frequency of UCR part II depends on slot

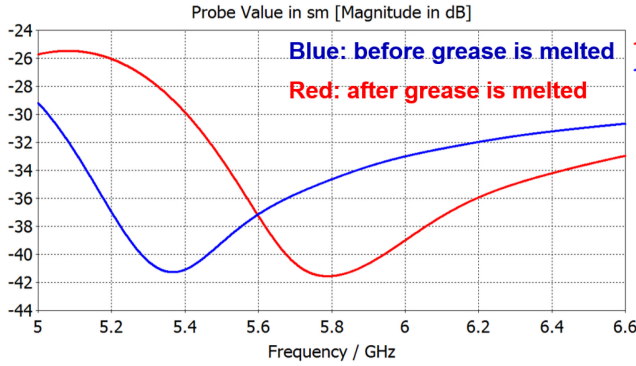


Fig. 6. Frequency response spectrum of UCR part II (temperature tracker).

parameters, substrate dielectric constant, and ambient temperature. To implement temperature tracking with memory, copper balls will be filled into the substrate of UCR part II. If the UCR tag has ever been exposed to a temperature higher than the melting point of grease, then the grease would be melted and the copper balls would fall down to the bottom. The positions of copper balls in the substrate will impact the distribution of electromagnetic field. Consequently, the resonance point of UCR part II will shift to either higher or lower frequency after grease is melted, as shown in Figure 6. The essential difference between our proposed temperature tracking approach and regular sensor-based temperature monitoring methods as reviewed in Section 2 is that our proposed temperature tracker has memory. In other words, the change of frequency response spectrum of UCR part II caused by ambient temperature variance is irreversible. When the ambient temperature returns to its normal level, the frequency response spectrum of UCR part II cannot be easily restored. Note that other than grease, many other different materials (e.g., ice, butter, animal fat, etc.) with varying melting points can be used to compose the substrate of UCR part II specific to different application requirements (i.e., different recommended storage temperatures for diverse commodities). Admittedly, mechanical fluctuations and vibrations during the transport may also change the positions of copper balls inside the substrate of UCR part II and thus shift the resonance point. Since RF signal can travel through paper and/or plastic package, a UCR tag can be placed inside the package of commodity. The impact of mechanical fluctuations and vibrations can be significantly reduced by introducing cushioning materials, which are commonly used to protect fragile commodities during the transport, to the packages of commodities. In addition, special materials that are only sensitive to temperature while insensitive to mechanical fluctuations and vibrations could be used as the substrate material of UCR part II to eliminate the impact of mechanical fluctuations and vibrations during the transport. The study of material properties is out of the scope of this article.

4.2 Look-up Method

As shown in Figure 3, during the *enrollment phase*, the signatures of all UCR tags ($\vec{v}_1, \vec{v}_2, \dots, \vec{v}_M$) are measured by the manufacturer. The Euclidean distance ($ED_{0,i}$) between the signature of design value (\vec{v}_0) and the signature of each tag (i.e., \vec{v}_i) will be computed and used as the analog index (AI) to look up that tag in the database. All the AIs will be sorted and a corresponding digital index (DI) will be assigned to each tag. All signatures of UCR tags will be appended to their DIs and AIs and stored in the look-up table as shown in Figure 7. During the *authentication phase*, we first calculate the Euclidean distance ($ED_{0,TUA}$) between the signature of design value (\vec{v}_0) and the signature of TUA (\vec{v}_{TUA}). $ED_{0,TUA}$ will be used to locate TUA on the AI axis as shown in Figure 7.

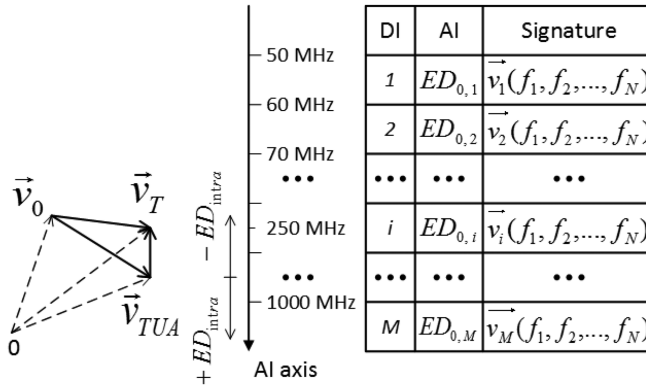


Fig. 7. Look-up table that stores all the signatures of valid tags.

Afterwards, we compare the signature of TUA with its nearest neighbor (i.e., Tag $DI(k)$ satisfying the condition that $|ED_{0,TUA} - ED_{0,DI(k)}|$ is the smallest) on the AI axis. This procedure will automatically terminate if the signature of TUA matches with its k_{th} nearest neighbor; otherwise, we move on to its $(k + 1)_{th}$ nearest neighbor. This procedure will also terminate if the shift value of TUA on the AI axis has exceeded the maximum intra-tag Euclidean distance (ED_{intra}), in which case we determine that TUA does not belong to the database. If the tag record (\vec{v}_T) that matches with TUA exists, then there is no chance for us to miss it because of the following triangle inequality:

$$|\vec{v}_T - \vec{v}_0| - |\vec{v}_{TUA} - \vec{v}_0| \leq |\vec{v}_T - \vec{v}_{TUA}| \leq ED_{intra}. \quad (2)$$

In other words, the AI distance (i.e., the distance on the AI axis) between TUA and possibly existing target tag, whose signature is \vec{v}_T , should not be larger than ED_{intra} . The procedure of the UCR tag authentication is described in Algorithm 1. Note that there will be only one tag satisfying the condition $|\vec{v}_{TUA} - \vec{v}_{DI(k)}| \leq ED_{intra}$, which is the target tag if it exists, so long as there is no overlapping between inter-tag and intra-tag Euclidean distance distributions. Admittedly, when the number of UCR tags is extremely large, it is possible that inter-tag and intra-tag Euclidean distance distributions will partially overlap with each other, in which case multiple tag records could match with TUA and the one nearest in Euclidean distance to TUA will be selected. This problem can also be overcome by increasing the feature space (i.e., the number of resonance points in the frequency spectrum) of UCR tags. Compared with exhaustive search, we noticeably reduce the look-up time (i.e., the time consumed to find a matching between TUA and database entry).

4.3 Application Scenario

Figure 8 illustrates the communication flow in the real application scenario. For electronic product, UCR tag can be integrated on the PCB. For non-electronic product, UCR tag can be placed inside the package (e.g., on the backside of bottle cap). An RFID reader or a smart phone that integrates necessary hardware (i.e., antenna, analog front-end, analog-to-digital converter, etc.) can be used to read UCR tag and download tag-related information from the centralized database. Table 3 shows the database structure. The communication flow of UCR system is as follows:

Step 1: A reader (RFID reader or smart phone) stimulates the UCR tag with an UWB plane wave.

Step 2: The reader captures the unique ID and/or temperature signature of UCR tag.

Step 3: The reader sends the unique ID and/or temperature signature to the centralized database for authentication.

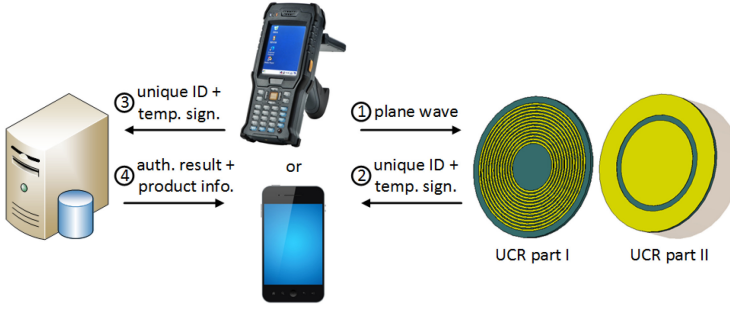


Fig. 8. Communication flow in real application scenario.

Table 3. Database Structure

DI	AI	Unique ID	Temperature Signature	Product Information
i	$ED_{0,i}$	$\vec{v}_i(f_1, f_2, \dots, f_N)$	f_{N+1}^i	1. Manufacturer 2. Ingredients 3. Product description 4. Expiration date

ALGORITHM 1: UCR tag authentication

```

1: procedure AUTHENTICATE( $\vec{v}_{TUA}$ )
2:    $\vec{v}_{TUA} \leftarrow$  The signature of TUA
3:    $\vec{v}_{DI(k)} \leftarrow$  The signature of TUA's  $k_{th}$  nearest neighbor on the AI axis, whose DI is  $DI(k)$ 
4:    $ED_{0,TUA} \leftarrow$  The Euclidean distance b/w design value and TUA
5:    $ED_{0,DI(k)} \leftarrow$  The Euclidean distance b/w design value and TUA's  $k_{th}$  nearest neighbor on the AI axis
6:   while  $|ED_{0,TUA} - ED_{0,DI(k)}| \leq ED_{intra}$  do
7:     if  $|\vec{v}_{TUA} - \vec{v}_{DI(k)}| \leq ED_{intra}$  then
8:       printf("TUA matches with Tag %d.",  $DI(k)$ )
9:       goto 11
10:    else
11:       $k \leftarrow k + 1$ 
12:    end
13:  end
14:  printf("TUA does not belong to the database.")
15: end procedure

```

Step 4: The centralized database sends the authentication result and corresponding product information (e.g., manufacturer, ingredients, product description, expiration date, etc.) to the reader.

Appending a tag unenrollment phase (i.e., removing tag signature from the database) to the last stage of the supply chain is optional for some particular applications and may prevent illegal tag recycling. But this also prevents the customer from authenticating the tag.

5 ADVERSARIAL MODEL

Assumption. We have two basic assumptions: (i) We assume that all authentic commodities must carry legal UCR tags to pass the authentication of authorized readers on the distribution path. (ii) We assume that the UCR tags of different commodities cannot easily be swapped. This is a

fair assumption taking into consideration that RF signal can travel through paper and/or plastic package and thus UCR tag can be placed inside the package of commodity without impacting access.

Adversary. Potential adversary could be any untrusted participant in the supply chain.

Goals of the Adversary. The adversarial goals we are addressing here include (i) injecting counterfeit commodities into the supply chain without detection by an authorized reader and (ii) preserving commodities sensitive to temperature at different temperatures other than what is required by the policy and attempting to hide this illicit behavior.

Capabilities of the Adversary. The adversary may perform any of the following actions against UCR system when commodities are distributed in the supply chain:

- *Reading:* The adversary may gain physical access to an authentic commodity carrying a legal UCR tag and capture the backscattered frequency response spectrum by stimulating the UCR tag using an UWB plane wave. The adversary must possess an appropriate reader to perform read operations.
- *Eavesdropping:* The adversary may eavesdrop on the RF channel to intercept the frequency response spectrum being backscattered from a legal UCR tag to an authorized reader.
- *Replaying:* The adversary may replay the intercepted frequency spectrum to an authorized reader to impersonate a legal UCR tag.
- *Cloning:* The adversary may accurately measure the physical parameters (i.e., geometric dimensions, dielectric constants of substrate materials, etc.) of legal UCR tags and try to fabricate duplicates.
- *Restoring:* The adversary may try to restore the initial positions of copper balls inside UCR part II.

We assume that the adversary is, however, restricted in one key aspect:

- *No access to the centralized database:* The adversary cannot read or modify data stored in the centralized database. This is a fair assumption, since the database is always protected with strong authentication protocols.

6 EVALUATION

In this section, we present the experimental setup and results. Simulation results based on CST Microwave Studio 2015 were presented in an earlier version of this article [34]. If the storage space of the centralized database is large enough, then there would be no limitation on the number of bits that could be used to represent each resonance point. The frequency band used by UCR tags is ultra-wideband (i.e., 3.1 to 10.6GHz). The resolution of measuring equipment used in our experiment is as small as tens of hertz. The analog value of each resonance point is actually represented by 36 bits. The standard deviations of resonance frequencies of 100 tag samples generated using pseudo random number generators have been shown in Table IV in the conference version [34] of this article. 6σ correspond to over one hundred MHz, which means that 28 bits out of 36 bits will vary if the analog value of resonance point is directly converted to binary without quantization. Since the tag signature is composed of 10 resonance points, the corresponding bit length would be 280 bits. Here, we evaluate the performance of manufactured UCR tags in terms of uniqueness and reliability. We also discuss how to increase the detection accuracy using machine-learning algorithms. Afterwards, we analyze the resilience of UCR system to the potential attacks. Lastly, we compare our proposed UCR system with the state-of-the-art techniques.

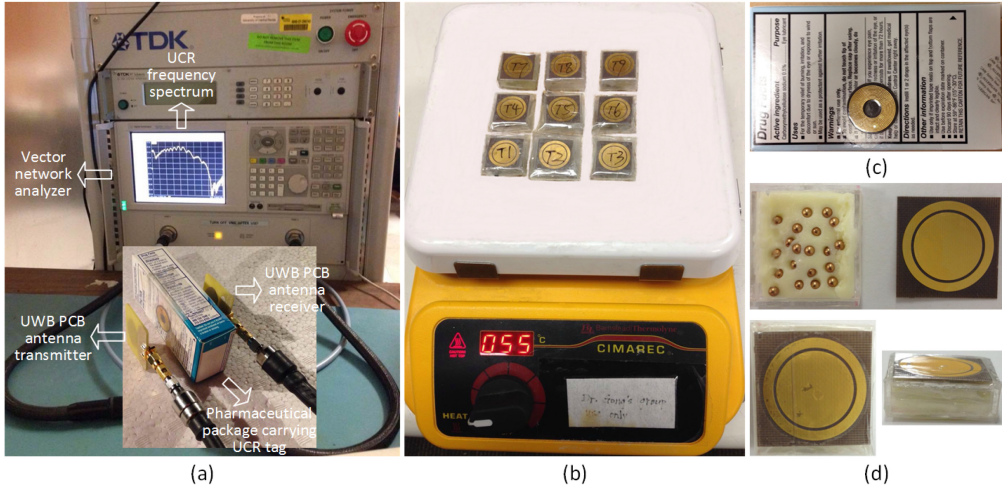


Fig. 9. (a) Experimental setup, (b) Barnstead Thermolyne hotplate, (c) UCR part I prototype attached to a pharmaceutical package, and (d) UCR part II prototype.

6.1 Experimental Setup

We use Agilent E8361A programmable network analyzer (PNA) to measure the insertion loss (S_{21}) of each UCR tag. Figure 9(a) illustrates the experimental setup. One UWB PCB antenna connected to port I of network analyzer will work as the transmitter and be responsible for stimulating the UCR tag with an UWB plane wave. Another UWB PCB antenna connected to port II of network analyzer will work as the receiver and be responsible for capturing the frequency response spectrum of UCR tag. The distance between the transmitter and the receiver is set to 10cm. The UCR tag is attached to a pharmaceutical package, which is placed in between the transmitter and the receiver, to mimic the real scenario. The Barnstead Thermolyne hotplate, as shown in Figure 9(b), is used to heat UCR part II and melt its substrate (butter in our prototype). Figure 9(c) and Figure 9(d) respectively illustrate the prototypes of UCR part I and II. UCR part I consists of 10 concentric ring slot resonators integrated on the TACONIC TLX-0 laminate. The metallic pattern is made of pure copper. The layout of UCR part I is shown in Figure 10(a). Table 4 lists its design parameters. UCR part II is a stand-alone circular ring slot resonator placed on two layers of substrates. The first layer of substrate is also made of TACONIC TLX-0 and its thickness is set to 0.254mm (the thinnest available thickness). The second layer of substrate is made of butter with 25 copper balls filled in. The butter is packaged with glass plates. The layout of UCR part II is shown in Figure 10(b). Table 5 lists its design parameters. The frequency band used by UCR tags ranges from 4 to 10GHz.

6.2 Performance Evaluation of UCR Part I

6.2.1 Euclidean Distance-Based Tag Recognition. In this subsection, we analyze the effectiveness of Euclidean distance-based tag recognition in the presence of environmental noise and with varying angles of incident plane wave. Fourteen UCR tags were measured 5 times at different conditions. Figure 12(a) illustrates the inter-tag and intra-tag Euclidean distance distributions of UCR tags in the presence of environmental noise. The margin between minimum inter-tag Euclidean distance and maximum intra-tag Euclidean distance reaches approximately 13.102MHz. Figure 12(b) shows the inter-tag and intra-tag Euclidean distance distributions of UCR tags when the angle of incident plane wave (see Figure 11) varies from 0° to 15° . The margin between minimum inter-tag Euclidean distance and maximum intra-tag Euclidean distance reaches approximately

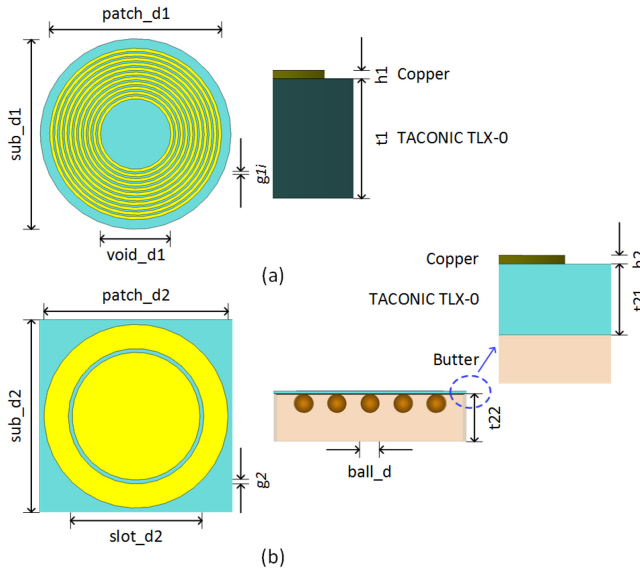


Fig. 10. (a) Layout of UCR part I and (b) layout of UCR part II.

Table 4. Design Parameters for UCR Part I

Variable	Parameter	Value
sub_d_1	Substrate diameter	20mm
t_1	Substrate thickness	0.5mm
ϵ_r	Substrate dielectric constant	2.45
$patch_d_1$	Patch diameter	18mm
h_1	Patch thickness	0.035mm
$void_d_1$	Central void diameter	7.4mm
g_{1i}	Air gap i ($i=1, \dots, 10$)	0.2mm

20.879MHz. To achieve high accuracy of tag recognition, the varying angle of incident plane wave should be not larger than 15° . Otherwise, there can be false negatives. The probability for a false positive would be negligible and much smaller than the probability for a false negative when the varying angle is larger than 15° . During the tag recognition phase, the varying angle of the incident plane wave could be regarded as an unpredictable and quasi-random disturbance. Different parts of the tag frequency spectrum information (i.e., amplitudes and phases at different frequency points) would shift towards different directions because of this disturbance. The probability that the vast majority of tag frequency spectrum information would shift towards the direction that is most beneficial for reducing the distance between two different tag signatures is negligible. Experimental result demonstrates that the Euclidean distances between signatures of UCR tags are effective at differentiating each other. Additional entropy can be acquired by integrating more slot resonators on the tag substrate or introducing more randomness to the electrical properties of tag substrate. For example, nano particles of random quantity with random diameters could be filled in random positions of tag substrate to introduce more randomness to the electrical property of tag substrate.

6.2.2 Machine-Learning-Based Tag Recognition. In this subsection, we analyze the effectiveness of machine-learning-based tag recognition. Supervised machine-learning techniques are utilized

Table 5. Design Parameters for UCR Part II

Variable	Parameter	Value
sub_d_2	Substrate diameter	20mm
t_{21}	Substrate I thickness	0.254mm
t_{22}	Substrate II thickness	5mm
ϵ_r	Substrate dielectric constant	2.45
$patch_d_2$	Patch diameter	19mm
h_2	Patch thickness	0.035mm
$slot_d_2$	Slot diameter	14mm
g_2	Air gap	0.5mm
$ball_d$	Copper ball diameter	2mm

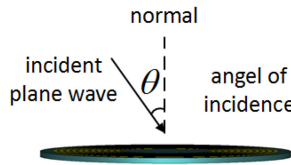
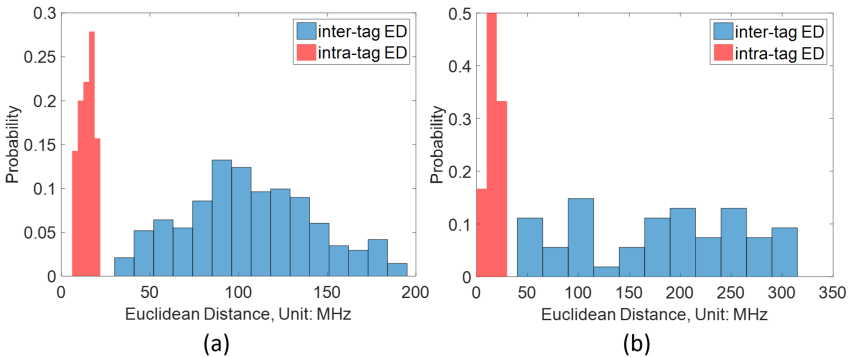


Fig. 11. Angle of incidence.

Fig. 12. (a) Euclidean distance distributions of UCR tags in the presence of environmental noise and (b) Euclidean distance distributions of UCR tags when angle of incidence varies from 0° to 15° .

to maximize the accuracy of tag recognition. Specifically, linear discriminant analysis (LDA) [17] is chosen due to its ability to focus on the most discriminating features between classes as opposed to the most expressive ones. Prior to any implementation it is important to first apply some pre-processing to the signals. In practice various noise sources may affect the locations of resonance points of UCR tags. Since these resonance points are frequency-domain characteristics, signal smoothing via a moving average filter is the best approach to ensure a quality signal spectrum that can be used for classification.

To continue, performing LDA on the sampled data requires a large amount of computations due to the high dimensionality of the signal. To solve this problem, principal component analysis (PCA) [27] is used not only to reduce dimensionality but also as a means of further noise removal. When applying PCA, the principal components were chosen in a manner to ensure that at least 95% of the total variance of the signal was maintained after projection to the new reduced dimensional space.

Table 6. Recognition Performance Comparison among Different PCA Training Partitions

Sampling resolution	Training size	Raw score (%)		Filtered score (%)	
		5 tags	10 tags	5 tags	10 tags
400	4	88	92.58	89.16	94.36
400	8	96.57	98.23	97.53	98.78
400	15	94.09	95.99	96.14	97.96
128,000	4	85.6	84.09	86.31	94.18
128,000	8	91.2	93.62	95.16	98.33
128,000	15	82.96	92.238	85.72	96.1

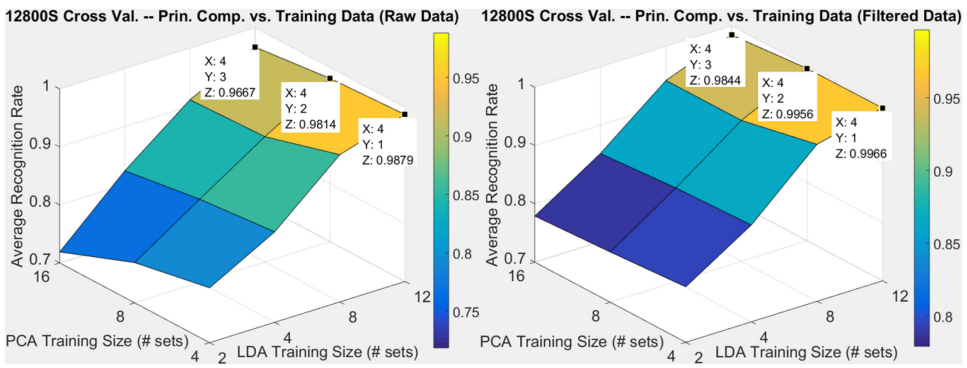


Fig. 13. Overall recognition performance for (30T, 15M, 12800S).

Additionally, both PCA and LDA processes were holistically evaluated through cross-validation. The parameters that were cross-validated were the amount of data used for calculating the principal components and training the classifier, as well as the different combinations of the training sets that were used, since some combinations of datasets may outperform others.

In particular, during the experimentation process there were multiple measurements gathered for different sets of tags and based on the amount of measurements the data was partitioned differently for training. For example, when 5 tags were measured 15 separate times the partitioning for PCA cross-validation was using 4 sets, 8 sets, and 15 sets of measurements for the 5 tags in different sequential combinations for computing the principal components for projection. For instance, in the case of 4 sets, the combinations tested for PCA were sets 1-4, 2-5, 3-6, and so on.

Then the projected data was used to train the LDA classifier by using partitions of 2 datasets (1-2, 2-3, etc.), 4 datasets (1-4, 2-5, etc.), 8 datasets (1-8, etc.) and 12 datasets. This results in 13, 11, 7, and 3 sets of test data that the classifier was not trained on for evaluating the classifier’s performance. Additionally, this cross-validation process was applied to tags with sampling frequencies of 400, 12,800, and 16,000 samples per signal. This not only offers understanding about which grouping of parameters may be optimal for training but also provides insight into the effects sampling resolution may have on classification performance. Table 6 displays this improvement for the LDA classifier trained on 12 sets of the data with different PCA training partitions. This demonstrates that the supervised learning technique not only accurately classifies tags but can maintain or even improve accuracy as the scale of the amount of tags increases.

Figure 13 shows the overall recognition performance for 30 tags. Each tag was measured 15 times with 12,800 sampling points. It is observed that the recognition performance maintains for

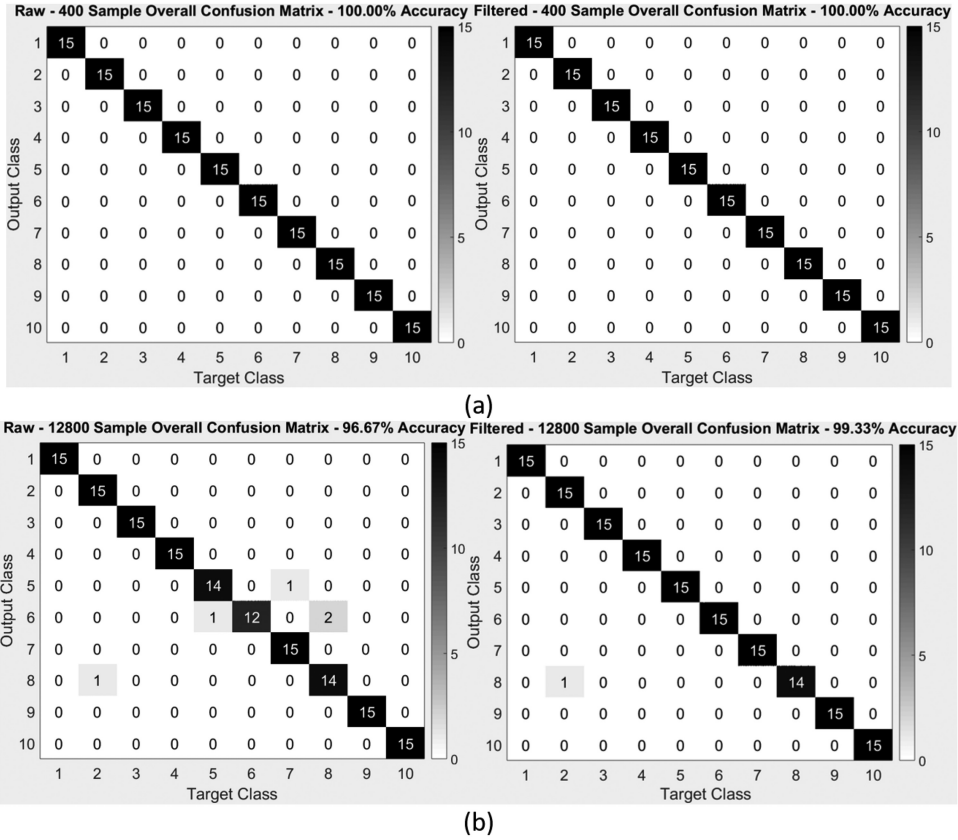


Fig. 14. (a) Overall confusion matrix for (10T, 15M, 400S) and (b) overall confusion matrix for (10T, 15M, 12800S).

a larger dataset. Top performing partitions for both raw and filtered datasets reach a recognition rate close to 100%. The lowest recognition rates for the raw and filtered datasets are 96.67% and 98.44% on average of all the different partitions and combinations.

To further solidify these results the optimal parameters for cross-validation were tested by being applied to the 400-sampling-point and 12,800-sampling-point datasets but with a random starting partition for training. This illustrates the effectiveness of using these parameters for training the classifier, since the previous results were the mean performance for combinations of different datasets. The random starting location should show that no matter what data the algorithm uses for training, the performance should be consistent with the results from cross-validation as long as enough variance of tag spectrum is represented in the data. Figure 14(a) and Figure 14(b) are the confusion matrices that display the classification results for the 10 tag-15 measurement-400/12,800 sampling-point experiments for a random starting location for training. As can be seen from the plots there were no misclassifications for the 400-sampling-point signals and only 6 misclassifications for the 12,800-sampling-point signal (5-row and 1-filtered). These results further reinforce the optimal parameters for cross-validation of 8 datasets for PCA training and 12 datasets for LDA training and the effectiveness of the supervised learning technique for classifying these UCR tags.

While this supervised classification method works very well for raw and filtered signals, as well as tags measured at different angles, the computational complexity required to compute the

Table 7. Unsupervised Recognition Performance Comparison for (20T, 30M, 12800S)

Classification Technique	Recognition Rate (%)	Response Time (ms)
Euclidean Distance	92.12	3.3
Normalized Correlation	91.97	2.1
Lorentzian Distance	91.33	0.106
Manhattan Distance	96.06	3.6
Dynamic Time Warping	100	5.1
Wavelet Transform Manhattan Distance	100	45.3

classifier can quickly increase in terms of scale depending on the number of tags that need to be enrolled in the database. Therefore, it is important to also look at various unsupervised methods of classification (i.e., non-machine-learning-based methods) that can effectively complete the same desired task. The resonance points of each tag are the designed discriminant features that are unique to each tag so naturally these features should be used as the feature vectors for each tag. For these experiments the resonance points were located using a valley detection algorithm in the bandwidth of 4.1GHz to 9.4GHz, since this is the bandwidth of interest for the resonance points. However, since the valley detection technique relies on the detection of local minima the raw signal must be effectively pre-processed first to ensure the proper location of the resonance points as local minima and minimize any false minima detection. The pre-processing consists of the smoothing used during the supervised learning process. The optimal window size for searching for a resonance point was empirically determined to be 5 times the length of the window used in the moving average filter during pre-processing. After the resonance points have been located, classification will simply depend on computing the distance/similarity between tag measurements and selecting the smallest distance between tag instances or the highest similarity score depending on the technique used.

To effectively evaluate the performance of unsupervised classification, multiple distance measures were used, including Euclidean, Manhattan, Lorentzian, and the normalized correlation coefficient. Furthermore, unsupervised classification that does not require explicitly locating resonance points was explored as well by using techniques such as dynamic time warping [28] and computing the Manhattan distance between two tag measurements after performing wavelet transformation [2] and comparing the resultant coefficients. Dynamic time warping is useful for classification in this regard, because although we may be dealing with signals in frequency domain instead of time domain, the features of interest are the locations of the resonance points and a similarity comparison between vectors can be done effectively using this technique. It effectively uses the resonance points as the features of interest without the need to explicitly search for them prior to classification. The specific wavelet chosen for classification was the Haar wavelet, since it is adept at detecting abrupt discontinuities in a spectrum. After obtaining the wavelet transform coefficients of two tag measurements, the Manhattan distance between tags' wavelet coefficients was computed and resulted in an 8×8 matrix and the sum of the diagonals across this matrix was used to determine similarity between tag measurements. The minimum diagonal distance sum was determined to effectively represent the correct tag identification. Table 7 compares different unsupervised methods in terms of recognition performance for (20T, 30M, 12800S). Similar to the cross-validation process used in training the linear discriminant classifier, the tags were evaluated by selecting a group of tags from a set of measurements to serve as the gallery (enrolled) set and then use the remaining tags to serve as the probe (verification) sets. The performance is evaluated holistically so each measurement group serves as a gallery at least once and as probes the rest of the time.

Table 8. Unsupervised Recognition Performance Comparison for (8T, 6A, 5M, 8000S)

Classification Technique	Recognition Rate (%)	Response Time (ms)
Euclidean Distance	97.33	9.5
Normalized Correlation	93	5
Lorentzian Distance	90.42	0.224
Manhattan Distance	98.75	8.4
Dynamic Time Warping	100	7.7
Wavelet Transform Manhattan Distance	99.92	73.7

As shown in Table 7, a maximum recognition rate of 100% was achieved for both the dynamic time warping and wavelet transform method. Dynamic time warping and wavelet transformation performed the best due to neither relying on the explicit locating of resonance points to use in the feature vector prior to classification. Since the other techniques do rely on this, there is room for inaccuracies during local minima detection that can lead to incorrect distance calculations and classification results. Additionally, these results are likely directly influenced by the fact that the original signals obtained in this dataset had minimal ambient noise interference and went through significant pre-processing. Therefore, these unsupervised methods of classification are comparable to the supervised LDA method when the measurement and processing conditions are almost optimal. However, it is also apparent that the supervised method is a more robust method, since the average recognition rates of the raw signal datasets are often comparable to the filtered signal datasets by most times only a few percentage points. As a tradeoff for better recognition accuracy, wavelet transform method does require a longer average response time because of larger amount of computation. Dynamic time warping achieves the best balance between recognition accuracy and average response time.

To effectively evaluate the performance of these unsupervised classification techniques, they were applied to the tags measured at different angles of incidence. By evaluating the tag measurements with varying angles of incidence, it is observed that as long as the tag is enrolled at all proper angles, it can be accurately identified during the verification stage via a simple unsupervised classification method. The same unsupervised techniques and evaluation methods were used as the tags measured at the same angle earlier and the results are shown in Table 8.

The frequency spectrum of UCR tag is susceptible to the angle of incidence of plane wave. Naturally, this could cause some issues in terms of classification, since the tags are classified based on their respective spectra and locations of their resonance points. To ensure that the reliability of UCR tag is not vulnerable to variance of reading angle and that the classification algorithm is robust enough to handle this variance, 8 tags measured at 6 different angles of incidence (i.e., 0°, 5°, 10°, 15°, 20°, and 25°) were tested. Each tag was measured 5 times for each reading angle. Once again the same testing and cross-validation process was used to evaluate how truly robust the tags and classification algorithms were in terms of recognition but now the partitions used for training were 1 to 5 measurement sets for computing the principal components and 2 to 3 measurement sets for training the LDA classifier. For the raw dataset with varying angles of incidence, the lowest recognition score achieved was 76% when using 5 sets for PCA training and 2 sets for LDA training. The top performing recognition score for the raw datasets was 89.58% when using 1 set to train PCA classifier and 5 sets to train LDA classifier. The filtered dataset performed much better with a minimum average recognition rate of 99.25% and a maximum average recognition rate of 100% for the same partitions as the raw dataset. This shows that although variance of reading angle likely adds some noise to the captured frequency spectrum, proper pre-processing can help minimize its impact. Table 8 compares the recognition performance of different unsupervised classification

Table 9. Resonance Point Shift after Exposed to a High Temperature

Tag	LT		HT		Δ_1 / MHz	Δ_2 / MHz
	mean(f_1)/GHz	mean(f_2)/GHz	mean(f_1)/GHz	mean(f_2)/GHz		
1	4.2679	7.2113	4.4214	6.8083	153.4688	-403.0313
2	4.2143	7.3680	4.3395	7.6635	125.1563	295.5
3	4.9313	6.7684	4.328	5.8983	-603.2813	-870.0938
4	4.2234	7.5563	4.4795	5.7199	256.125	-1836.4
5	4.2557	7.3689	4.4087	5.9851	153	-1383.8
6	4.2953	7.2675	4.451	7.1031	155.7188	-164.3438
7	4.6707	7.2314	4.6118	7.6194	-58.875	388.0313
8	4.408	7.0641	4.3737	7.4688	34.3125	404.625
9	4.4603	7.5044	4.4351	7.518	-25.2188	13.5938

techniques for the dataset of 8 tags-6 reading angles for each tag-5 measurements for angle-8000 sampling points for each measurement. With all methods scoring above 90% recognition accuracy, this reinforces the ability to use these techniques for tag identification with decreased computational complexity. Although these scores outperformed the supervised classification of the raw signals, they were still on average lower than the worst performing filtered supervised classification results. Again, wavelet transform method requires the longest average response time because of the largest amount of required computation. Dynamic time warping achieves the best balance between recognition accuracy and average response time.

6.3 Performance Evaluation of UCR Part II

In this subsection, we evaluate the performance of UCR part II in terms of tracking temperature. 9 UCR tags were measured 10 times both before and after exposed to a high temperature. The Barnstead Thermolyne hotplate, as shown in Figure 9(b), was used to heat UCR part II and melt its substrate (butter in our prototype). Table 9 shows the shifts of both first-order (1st-order) and second-order (2nd-order) resonance points. LT and HT, respectively, denote low temperature and high temperature. f_1 and f_2 respectively indicate 1st-order and 2nd-order resonance points. $mean(X)$ represents the mean value out of 10 measurements. Δ_1 and Δ_2 respectively indicate the shifts of 1st-order and 2nd-order resonance points after exposed to a high temperature.

As shown in Figure 2(c), the first-order partial derivative of notch frequency with respect to dielectric constant of substrate material is larger than zero in the UWB, which means that the larger the dielectric constant of substrate material is, the larger the notch frequency will be. When the contrast ratio between the dielectric constants of the background and inclusions is small, the effective dielectric constant of the composite material depends on the volume fraction occupied by the inclusions and is not affected by the inhomogeneities distribution [26]. When this contrast ratio becomes large, the effective dielectric constant of the composite material would also depend on the component arrangement in space [26]. The dielectric constant of copper is 1. The dielectric constant of unsalted butter is 24.5 when measured at 30°C and 2450MHz [1]. Since the contrast ratio between the dielectric constants of butter and copper is very large (larger than 20), the effective dielectric constant of the substrate of UCR part II would be impacted by the spatial distribution of copper balls inside the butter. Since both before and after exposed to a high temperature, the positions of copper balls inside the butter are random. The effective dielectric constant of the substrate of UCR part II and thus its resonance frequency could become either larger or smaller after exposed to a high temperature. So long as the ambient temperature is below the melting point of substrate material of UCR part II, the substrate would not melt and the positions of coppers

would not change. Therefore, when the tag is exposed to temperatures in between low and high temperatures, the frequency response would be the same as the frequency response tested under low temperature. Experimental result demonstrates that UCR part II is effective at tracking temperature with memory.

6.4 Attack Analysis

In this subsection, we evaluate the resilience of UCR system towards potential attacks. UCR system is resistant to cloning attack, since the adversaries cannot easily model the uncontrollable process variations during tag fabrication. UCR system is intrinsically resistant to DoS attack performed in the form of overwriting tag memory, since tag memory has been eliminated from the UCR system. UCR system builds up the trustworthy visibility into supply-chain status by providing a unique, reliable and unclonable identifier for commodity track-and-trace and integrating an irreversible temperature tracker to record temperature-related history information. Exposure to high temperature cannot be hidden, since the adversary cannot easily restore the initial positions of copper balls without destroying the package of UCR tag. As a result, non-repudiation is available when multiple parties are involved in the supply chain and one intermediate supply-chain participant finds out that the commodities haven't been kept refrigerated as required by the previous stage. Admittedly, the adversaries could record the frequency response spectrum of one UCR tag and replay the frequency response when a forged tag is being stimulated. However, this type of replay attack needs an extra apparatus to replay the frequency response, which will be too expensive to be a realistic attack to the supply chain of low-cost commodities. Like many other existing RFID-based solutions, UCR system is susceptible to RF interference. This issue can be addressed by repeating measurements of UCR tags provided that most of the time the appearance of RF interference is intermittent. UCR system is also susceptible to split attacks (i.e., separating tag from product, swapping tags, etc.), which will be addressed in our future work. Admittedly, if an attacker overbuilds UCR tags, he/she may possibly find a few tags the Euclidean distances between which are quite small. However, taking into consideration that UCR tags are mainly designed to track and trace low-cost non-electronic products (expensive electronic products could be protected by the IC-based RFID solution), this type of attack may not be practically economically attractive for the attacker. The attacker may have to overbuild millions of UCR tags to find a few the ED values between which are quite small. The potential economic returns could be only tens of dollars while the attack cost could be even higher. The probability of finding UCR tags with similar signatures by overbuilding could be significantly reduced by enlarging the feature space of tag signature. One simple way is to integrate more slot resonators on the tag substrate.

6.5 Comparison with Prior Work

Table 10 compares UCR with prior work in terms of overhead (e.g., tag area), capacity (e.g., ID size), and security (e.g., unclonability), and so on. Although the authors in Reference [9] also use one analog feature (the delay between the structural and tag modes) as the identifier, their proposed identifier is still clonable simply because the resolution of delay difference (100ps) is not small enough. In contrast, the resolution of resonance frequency difference in UCR system depends on the number of sampling points and can be as small as 0.5Hz. Although the chipless RFID tag proposed in Reference [9] integrates a temperature sensor that modulates the amplitude of the backscattered signal as a function of the temperature, this temperature-sensing mechanism is reversible and cannot simply be adapted to track the temperatures of commodities in the supply chain due to the lack of memory. As discussed in Section 6.4, UCR system enables non-repudiation of previous exposure to high temperature. UCR tag is believed to be low-cost because of printability, small ID size, and no requirement for post-processing.

Table 10. Comparison with Prior Work

Metrics	Stevan et al. [20]	Md. Aminul et al. [16]	David et al. [9]	GOST [13]	UCR
Based on	FD	FD	TD	TD	FD
Tag area	88mm × 65mm	7.2mm × 5.8mm × 4	13.65cm × 10cm	N/A	20mm × 20mm × 2
ID size	35 bits	16 bits	1 analog value	64 bits	10 analog values
Unclonability	×	×	×	×	√
Temperature sensing	×	×	√	×	√
Irreversible temperature tracking	×	×	×	×	√
Printability	√	√	√	×	√
Post-processing	Yes	Yes	No	No	No

Note: 1. FD and TD respectively indicate frequency domain and time domain.

2. Post-processing indicates the process of layout modification after fabrication in the form of spiral shorting or removing.

7 CONCLUSION AND FUTURE WORK

In this article, we presented a new unclonable, environmentally sensitive chipless RFID (UCR) tag that carries a unique ID and enables irreversible temperature tracking. The effectiveness of UCR system in terms of tag recognition and temperature tracking has been verified via experiments based on UCR prototypes. UCR system not only builds up dependable visibility into supply-chain status but also has the potential to enlarge the scope of the IoT by enabling many non-electronic products to be connected to the network. UCR tags can be attached to the packages of products, integrated onto the PCBs of electronic products, or printed on the products or their packages with conductive 3D printing materials. Compared with existing approaches, UCR system has the following advantages: (1) The ID provided by UCR tag is unique and unclonable, since it depends on the random and uncontrollable process variations during tag fabrication; (2) UCR tags can be fabricated with the same layout and do not require post-processing (i.e., removing or shorting some of the resonators that construct the chipless RFID tag) to encode data, which significantly reduces the manufacturing time/cost; (3) UCR tags have the capability to track the temperatures of commodities in the supply chain and help preserve the cold chain for those commodities (e.g., vaccines, pharmaceuticals, etc.) sensitive to temperature; (4) Compared with exhaustive search, our proposed look-up method remarkably accelerates the authentication process of UCR tags. In future work, we plan to develop a pill/capsule-level track-and-trace technique.

REFERENCES

- [1] Jasim Ahmed, Hosahalli S. Ramaswamy, and Vijaya G. S. Raghavan. 2007. Dielectric properties of butter in the MW frequency range as affected by salt and temperature. *J. Food Eng.* 82, 3 (2007), 351–358.
- [2] Ali N. Akansu, Wouter A. Serdijn, and Ivan W. Selesnick. 2010. Emerging applications of wavelets: A review. *Phys. Commun.* 3, 1 (2010), 1–18.
- [3] Emran Md Amin and Nemai Karmakar. 2011. Development of a chipless RFID temperature sensor using cascaded spiral resonators. In *Proceedings of the 2011 IEEE Sensors*. IEEE, 554–557.
- [4] John Fredy Barrera, Alejandro Mira-Agudelo, and Roberto Torroba. 2014. Experimental QR code optical encryption: Noise-free data recovering. *Optics Lett.* 39, 10 (2014), 3074–3077.
- [5] Matt Cole. 2016. Cargo theft numbers down in 2015, FreightWatch reports. Retrieved from <http://www.OverdriveOnline.com/cargo-theft-numbers-down-in-2015-freightwatch-reports/>.
- [6] U.S. Customs and Border Protection. 2015. CBP, ICE HSI Report \$1.2 Billion in Counterfeit Seizures in 2014. Retrieved from <https://www.cbp.gov/newsroom/national-media-release/cbp-ice-hsi-report-12-billion-counterfeit-seizures-2014>.
- [7] Srinivas Devadas, Edward Suh, Sid Paral, Richard Sowell, Tom Ziola, and Vivek Khandelwal. 2008. Design and implementation of PUF-based “unclonable” RFID ICs for anti-counterfeiting and security applications. In *Proceedings of the 2008 IEEE International Conference on RFID*. IEEE, 58–64.

- [8] Martin Feldhofer, Sandra Dominikus, and Johannes Wolkerstorfer. 2004. Strong authentication for RFID systems using the AES algorithm. In *Proceedings of the International Workshop on Cryptographic Hardware and Embedded Systems*. Springer, 357–370.
- [9] David Girbau, Ángel Ramos, Antonio Lazaro, Sergi Rima, and Ramón Villarino. 2012. Passive wireless temperature sensor based on time-coded UWB chipless RFID tags. *IEEE Trans. Microw. Theory Techn.* 60, 11 (2012), 3623–3632.
- [10] Dong Sam Ha and Patrick R. Schaumont. 2007. Replacing cryptography with ultra wideband (UWB) modulation in secure RFID. In *Proceedings of the 2007 IEEE International Conference on RFID*. IEEE, 23–29.
- [11] Masahiro Hara, Motoaki Watabe, Tadao Nojiri, Takayuki Nagaya, and Yuji Uchiyama. 1998. Optically readable two-dimensional code and method and apparatus using the same. (March 10 1998). US Patent 5,726,435.
- [12] S. Härmä, V. P. Plessky, C. S. Hartmann, and W. Steichen. 2006. SAW RFID tag with reduced size. In *Proceedings of the 2006 IEEE Ultrasonics Symposium*. 2389–2392.
- [13] Clinton S. Hartmann. 2002. A global SAW ID tag with large data capacity. In *Proceedings of the 2002 IEEE Ultrasonics Symposium*, Vol. 1. IEEE, 65–69.
- [14] Daniel Hein, Johannes Wolkerstorfer, and Norbert Felber. 2008. ECC is ready for RFID—A proof in silicon. In *Proceedings of the International Workshop on Selected Areas in Cryptography*. Springer, 401–413.
- [15] Charles Herder, Meng-Day Yu, Farinaz Koushanfar, and Srinivas Devadas. 2014. Physical unclonable functions and applications: A tutorial. *Proc. IEEE* 102, 8 (2014), 1126–1141.
- [16] Md Aminul Islam and Nemai Chandra Karmakar. 2012. A novel compact printable dual-polarized chipless RFID system. *IEEE Trans. Microw. Theory Techn.* 60, 7 (2012), 2142–2151.
- [17] Alan Julian Izenman. 2013. Linear discriminant analysis. In *Modern Multivariate Statistical Techniques*. Springer, 237–280.
- [18] Arun Kanuparthi, Ramesh Karri, and Sateesh Addepalli. 2013. Hardware and embedded security in the context of internet of things. In *Proceedings of the 2013 ACM Workshop on Security, Privacy & Dependability for Cyber Vehicles*. ACM, 61–64.
- [19] Stevan Preradovic, Isaac Balbin, Nemai Chandra Karmakar, and Gerhard F. Swiegers. 2009. Multiresonator-based chipless RFID system for low-cost item tracking. *IEEE Trans. Microwave Theory Techn.* 57, 5 (2009), 1411–1419.
- [20] Stevan Preradovic and Nemai C. Karmakar. 2009. Design of fully printable planar chipless RFID transponder with 35-bit data capacity. In *Proceedings of the 2009 European Microwave Conference (EuMC 2009)*. IEEE, 013–016.
- [21] Stevan Preradovic and Nemai Chandra Karmakar. 2010. Chipless RFID: Bar code of the future. *IEEE Microw. Mag.* 11, 7 (2010), 87–97.
- [22] Stevan Preradovic and Nemai Chandra Karmakar. 2012. Chipless RFID tag. In *Multiresonator-Based Chipless RFID*. Springer, 77–94.
- [23] Associated Press. 2016. China arrests 135 for illegally buying, selling vaccines. Retrieved from <http://www.sandiegouniontribune.com/sdut-china-arrests-135-for-illegally-buying-selling-2016may20-story.html>.
- [24] Austin Ramzy. 2016. China Says It Found Ring Said to Sell Improperly Stored Vaccines. Retrieved from <https://www.nytimes.com/2016/03/22/world/asia/china-vaccine-sales.html>.
- [25] Ulrich Rührmair, Srinivas Devadas, and Farinaz Koushanfar. 2012. Security based on physical unclonability and disorder. In *Introduction to Hardware Security and Trust*. Springer, 65–102.
- [26] Bruno Sareni, Laurent Krähenbühl, Abderrahmane Beroual, and Christian Brosseau. 1997. Effective dielectric constant of random composite materials. *J. Appl. Phys.* 81, 5 (1997), 2375–2383.
- [27] Jonathon Shlens. 2014. A tutorial on principal component analysis. *arXiv Preprint arXiv:1404.1100* (2014).
- [28] Diego F. Silva and Gustavo E. A. P. A. Batista. 2016. Speeding up all-pairwise dynamic time warping matrix calculation. In *Proceedings of the 2016 SIAM International Conference on Data Mining*. SIAM, 837–845.
- [29] Arnaud Vena, Etienne Perret, Smail Tedjini, Darine Kaddour, Alexis Potie, and Thierry Barron. 2012. A compact chipless RFID tag with environment sensing capability. In *Proceedings of the 2012 IEEE MTT-S International Microwave Symposium Digest (MTT'12)*. IEEE, 1–3.
- [30] Charles Wankel. 2007. *21st Century Management: A Reference Handbook*. Sage Publications.
- [31] Rolf H. Weber and Romana Weber. 2010. *Internet of Things*. Vol. 12. Springer.
- [32] Norman J. Woodland and Silver Bernard. 1952. Classifying apparatus and method. (Oct. 7 1952). US Patent 2,612,994.
- [33] Kun Yang, Domenic Forte, and Mark M. Tehranipoor. 2015. Protecting endpoint devices in IoT supply chain. In *Proceedings of the 2015 IEEE/ACM International Conference on Computer-Aided Design (ICCAD'15)*. IEEE, 351–356.
- [34] Kun Yang, Domenic Forte, and Mark M. Tehranipoor. 2016. UCR: An unclonable chipless RFID tag. In *Proceedings of the 2016 IEEE International Symposium on Hardware Oriented Security and Trust (HOST'16)*. IEEE, 7–12.

Received June 2017; revised July 2018; accepted August 2018